

Toward Automatic Label-Free Whispering Gallery Modes Biodetection with a Quantum Dot-Coated Microsphere Population

M. Charlebois · A. Paquet · L. S. Verret · K. Boissinot ·
M. Boissinot · M. G. Bergeron · C. Nì. Allen

Received: 24 September 2009 / Accepted: 16 January 2010 / Published online: 20 February 2010
© The Author(s) 2010. This article is published with open access at Springerlink.com

Abstract We explore a new calibration-free approach to biodetection based on whispering gallery modes (WGMs) without a reference measure and relative shifts. Thus, the requirement to keep track of the sensor position is removed, and a freely moving population of fluorophore-doped polystyrene microspheres can now fulfill this role of sensing resonator. Breaking free from fixed surface-based biosensing promotes adhesion between the microsphere sensors and the analytes since both can now be thoroughly mixed. The 70-nm-wide spectrum of green fluorescent microbeads allows us to monitor over 20 WGMs simultaneously without needing evanescent light coupling into the microspheres, hence enabling remote sensing. Since the exact radius of each microsphere is unknown a priori, it requires algorithmic analyses to obtain a reliable result for the refractive index of a solution. We first test our approach with different solutions of alcohol in water obtaining 3×10^{-4} precision on the refractive index at lower concentrations. Then, the solutions of bacterial spores in water yield clear evidence of biodetection in the statistical analysis of WGMs from 50 microspheres. To extend the fluorescence spectral range of our WGM sensors, we present preliminary results on coating microspheres with CdSe/ZnS quantum dots.

Keywords Whispering gallery modes · Biodetection · Optical resonances · Morphology-dependant resonances · Refractometers · Microspheres · Sensors

Introduction

Dielectric microspheres can act as resonators with a geometry that offers the highest quality factor (Q up to 10^9) [1]. The light trapped in these resonators by means of total internal reflection exhibits very strong and sharp resonances, called whispering gallery modes (WGMs), at specific wavelengths known from Mie theory [2, 3]. In this formalism, these resonances are determined by the radius a of the microsphere and the refractive index contrast $m = m_1/m_0$ where m_1 and m_0 are the refractive indices of the microsphere and the surrounding medium, respectively. The microspheres can thus act as very sensitive refractometer sensors [4] or even biodetectors. The signal transduction mechanism for biodetection is typically the wavelength shift induced by evanescent field coupling between WGMs and analytes surrounding the microcavities [5–9], making it even possible to detect single binding events. All these absorption-based methods require precise evanescent coupling of the excitation source in a WGM. They thus suffer from relying on fragile fiber tapers, angled-polished fibers, coupling prisms, etc. with a critical dependence on their alignment.

In contrast, fluorescent microspheres can be used as microcavities with a simple incoherent or coherent remote illumination source to excite the fluorophores that will emit light coupling directly in the WGMs [10–20]. Zijlstra et al. showed that these microspheres can act as indirect refractometers without knowledge of the exact size of any individual microsphere, but the size distribution must still be

M. Charlebois · A. Paquet · L. S. Verret · C. Nì. Allen (✉)
Centre d'Optique, Photonique et Laser (COPL), Département de physique, de génie physique et d'optique, Université Laval,
Quebec, QC G1V 0A6, Canada
e-mail: claudine.allen@phy.ulaval.ca

K. Boissinot · M. Boissinot · M. G. Bergeron
Centre de Recherche en Infectiologie de l'Université Laval,
Centre Hospitalier Universitaire de Québec (Pavillon CHUL),
Quebec, QC G1V 4G2, Canada

measured in advance [11]. Weller et al. also report on finding the size of microspheres from the WGMs in their fluorescence spectra using analytical expressions from Oraevsky [3], but the experiments were limited to air ($\varepsilon = 1$) only and their analysis did not yield refractive index sensing simultaneously [10]. Another, less flexible, approach to refractometry is to pre-calibrate the WGM spectral displacements for each microsphere against solutions of known refractive indexes [21, 22]. This requires the microsphere position to be known and retraceable for any further refractive index measurement. The same concept of comparing WGM spectra from a fixed fluorescent microsphere has been applied in biosensing to follow DNA hybridization kinetics [13] and BSA adsorption kinetics [10, 23, 24].

In this letter, we propose a new absolute WGM-based sensing method that does not require calibration, reference measures or any prior knowledge about the microsphere radii. Only one spectrum acquisition per fluorescent microsphere is needed; hence, we no longer have to keep track of the position of each microsphere between manipulations. This opens up new engineering possibilities for sensor integration in fluidic systems (including microfluidics and lab-on-chip devices). In the case of biodetection, this method breaks free from surface-based sensing with poor analyte capture efficiencies and facilitates the mixing of microsphere sensors with analytes. After a brief overview of the experimental setup as well as the WGM theory as formulated by H. Chew [25, 26] and applied by Zijlstra et al. [11], a new algorithm will be exposed to analyze fluorescence emission spectra with multiple WGMs. Fitting the theoretical WGMs over the whole experimental spectral range ensures the finding of a unique combination (a, m_0) of microsphere radius and refractive index of the surroundings. We will show that the chosen theory, taking into account the dipole emitters within the microspheres and thus differing from the original Mie theory, and the chosen experimental conditions, where the microspheres are in suspension, yield an almost perfect match between the theoretical and experimental WGM spectra. Then, we test our algorithm using a microsphere population of radii unknown a priori to extract the refractive index of liquids. Also, results from applying our algorithm in label-free biodetection experiments will be discussed. Since free floating functionalized microspheres available commercially can now be directly used as fluorescent biodetectors, the sample preparation can be significantly simplified and shortened. Here, the analyte will be a dormant form of bacteria captured by a positively charged polymer coating on the microspheres and detected without a reference measurement. Finally, preliminary results on colloidal quantum dot (cQD) coated microspheres will be presented as a mean to improve WGM visibility and extend the

spectral range covered by fluorescence emission, eventually increasing the number of WGM fitted by our algorithm.

Fluorescent Microspheres

To determine the absolute value of the solution refractive index m_0 and microsphere radius a , multiple WGMs must be measured at the same time, as will be discussed later. A wide spectrum is thus necessary. The spectra from fluorophores embedded in microspheres can easily cover more than 100 nm. The emitted light from these microspheres is coupled more strongly into the WGMs, but the original Mie theory fails to correctly predict the scattered emission spectrum. This theory predicts the right WGM resonance wavelengths, but their relative intensity is better described by an elaboration of Mie theory (EMT) formulated by H. Chew [25, 26]. Simulations were performed based on this theory to find a suitable wavelength range and microsphere radius producing well-defined WGM resonances. These simulations were carried out with Matlab R2007a for Windows on a personal computer. EMT showed that increasing the radius of microspheres and the light frequency improves the Q factor. Since this factor is contravariant with free spectral range, a compromise is needed to maximize both. The 0.5-nm resolution of the spectrometer used limits the resolving power to distinguish two consecutive WGMs. The free spectral range must thus be wide enough to resolve experimentally every single WGM over the whole spectral range chosen. However, we must also keep the Q factor sufficiently high for good sensing precision. Based on these considerations and the commercial availability of water-soluble fluorescent polystyrene microspheres, we chose product G1000 (Duke Scientific Corporation) with a nominal radius of 4,950 nm and emission centered around 520 nm. The Q factor of these microbeads was measured with an Andor CCD camera and spectrometer having a resolution of 0.1 nm. This value is smaller than the FWHM of the WGM peaks giving a Q factor of $\simeq 2000$.

Experimental Setup

The core of our experimental setup reproduces a typical fluorescence microscope as illustrated in Fig. 1a. However, the configuration is not the usual epifluorescence one. The 488-nm argon laser beam, exciting the fluorescent microspheres, is transmitted through the microscope slide making an angle with the fluorescence propagation axis, so that only scattered laser light will co-propagate with the fluorescence. A 100X immersion oil microscope objective,

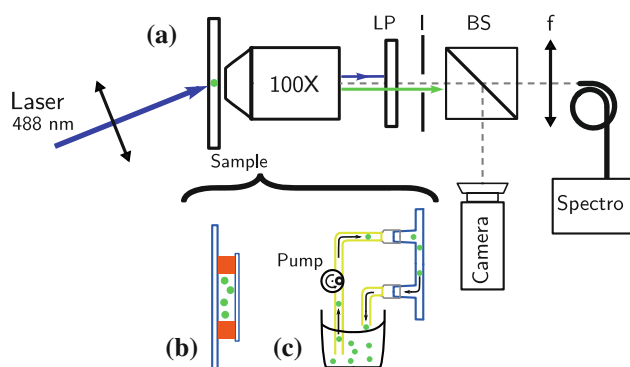


Fig. 1 **a** Fluorescence microscope. 100X : Oil immersion microscope objective, LP : longpass filter, I : variable iris, BS beam splitter, f : Coupling lens, Camera : CCD Pulnix, Spectro : Fiber spectrometer Ocean Optics. **b** 60 μ l sealed chamber with microspheres and fluid under analysis mounted on a microscope slide. **c** Microfluidics. A peristaltic pump circulates the solution through a microscope slide with a $0.4 \times 3.8 \times 17$ mm engraved channel

Olympus UPlan-FLN100XO2, collects the fluorescence on the other side of the slide, and a long-pass filter blocks the scattered laser light. The green fluorescence continues through a variable diaphragm that isolates the emission of a single microsphere. A beam splitter sends a portion of this emission to a camera to visualize the microsphere, and the remainder is injected into a fiber spectrometer Ocean Optics USB4000 to record the fluorescence spectrum modulated by amplified WGMs.

Two types of reservoir for fluids with microsphere sensors were used. The first tests were made with a SecureSealTM SA8R-1.0 chamber bonded on a microscope slide as pictured in Fig. 1b. This sealable chamber was filled with 60 μ l of a given solution. The typical sensor concentration in the solutions was around 950 microspheres/ μ l, since this was a good compromise to facilitate the measurement process. Single microspheres flowed frequently within the focal spot of the objective without touching the slide, but the probability of seeing multiple ones at the same time was still low. The second type of reservoir was a complete microfluidic apparatus, Fig. 1c. A peristaltic pump Watson-Marlow 400 circulated the solution in a closed loop including an IbiDi[®] μ -Slide inserted in the optical setup. This slide has a $0.4 \times 3.8 \times 17$ mm channel engraved with a ≈ 170 μ m thick wall on the imaging side. In this configuration, we can add, during same experiment, specific volumes of alcohols to vary the solution refractive index or add analytes at different concentrations to test the microspheres for biodetection.

Analysis Algorithm

Before comparing it with EMT, the acquired WGM spectrum of each single fluorescent microsphere must first be

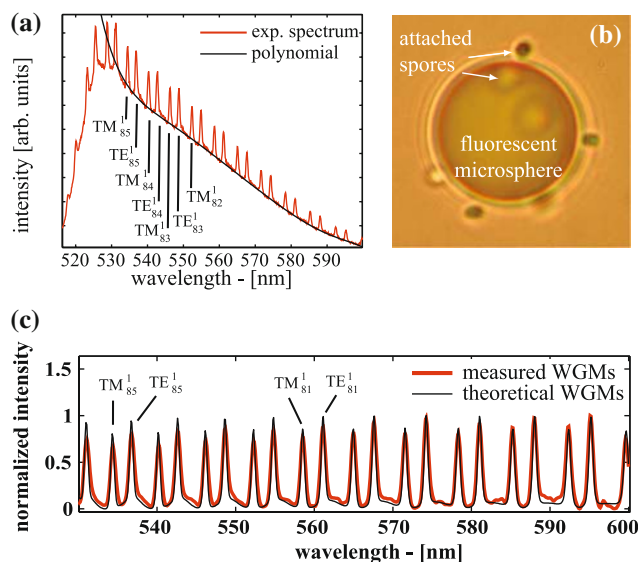


Fig. 2 **a** Smoothed fluorescence spectrum of a G1000 microsphere immersed in water with the *black line* indicating the polynomial used for background subtraction. **b** Image of a microsphere in water with spores adsorbed. The image is slightly defocused in order to see both the microsphere and spores. **c** Processed experimental spectrum (*red*) superimposed to the best fit of calculated EMT spectrum (*black*) displaying the near perfect agreement between theory and experiment

processed. After noise filtering, a seventh-order polynomial is fitted to the spectrum baseline to determine the fluorescence intensity, and then it is subtracted from the spectrum, see Fig. 2a. The resulting spectrum is then divided by the same polynomial in order to normalize the intensity of each WGM. The resulting spectrum spans 70 nm centered at 565 nm as seen in Fig. 2c and is now ready to be compared to EMT predictions.

Several theoretical spectra are calculated with Matlab algorithms in order to match the processed experimental spectrum. A typical least square algorithm cannot work automatically for multiple sharp peaks (such as WGMs) spectra, since it is an unstable procedure that usually requires a huge number of starting attempts to find the correct minimum. In order to proceed with such a fitting method, the starting parameters must thus be accurately determined first by a systematic, well-sampled rough scan of the parameter space. More precisely, a set of theoretical spectra is generated from EMT calculations for an ensemble of (a, m_0) parameters. The refractive index of polystyrene is known and given by the Sellmeier relation $m_1 = 1.5663 + 0.00785/\lambda^2 + 0.003478/\lambda^4$ (from Duke Scientific Corporation) where λ is the wavelength in nanometers. This set of theoretical spectra covers values of radius a from 4,800 to 5,000 nm and values of m_0 from 1.32 to 1.42 sampled at $\Delta a = 0.1$ nm and $\Delta m_0 = 0.0001$. Each calculated EMT spectrum associated to a (a, m_0) coordinate is sufficiently

sampled in wavelength ($\Delta\lambda = 0.02$ nm) to avoid incomplete delineation of sharp WGM peaks. A convolution with the instrumental line shape (FWHM = 0.5 nm) is then used to obtain a resolution matching the experimental data. This way, the energy contained in the extremely sharp WGMs is redistributed in a larger, shorter, Voigtian-like line profile, comparable with the experiment.

The processed experimental spectrum can now be compared to each calculated EMT spectrum with the least square approach. Calculating the squared sum of residuals between these spectra for each (a, m_0) generates a χ^2 map. Fig. 3b shows the global behavior of this map. Measuring and analyzing a single WGM peak would not yield the absolute minimum seen in this figure. Instead, we would obtain an infinite number of equivalent local minima with no possible distinction between them. The distinction becomes evident with 20 WGMs since the absolute minimum observed is a factor 2 lower than any other local minima, making the solution parameter set (a^*, m_0^*) unique, see the zoom on this absolute minimum in Fig. 3c. The origin of this distinction is presented in Fig. 3a that corresponds to the EMT spectrum calculated 60 nm away in radius from (a^*, m_0^*) . The spectral stretch induced by such a radius change causes the overall WGM pattern to be shifted on average by the distance between TM_l and TM_{l+1} WGMs where l is the azimuthal mode number. When comparing theoretical versus measured spectra in Fig. 3a, it is apparent that not all WGMs are accurately superposed in the full spectral range whereas the same comparison at (a^*, m_0^*) shown in Fig. 2c is near perfect. This ideal agreement is a consequence of working with EMT, which provides a more suitable formalism for fluorescent microspheres, and of our experimental conditions where the suspended microspheres do not lie on a substrate, hence m_0 is truly homogeneous.

Since the microsphere sample is polydisperse, no initial guess can be made about the radius coordinate a . Now that the initial rough scan has provided starting parameters very close to the absolute minimum, this fit can then be refined with a Levenberg-Marquardt algorithm [27] around (a^*, m_0^*) since the smooth χ^2 variation defines a relatively precise minimum. In order to converge to the absolute minimum, it has been noted that only one parameter must be fitted with the Levenberg-Marquardt algorithm. To do so, we fit only the radius a on a grid of m_0 which is 10 times more precise than the initial scan. The overall method converges automatically every time with near perfect agreement.

Refractive Index Sensing

To test the accuracy of our method, we prepared solutions of microspheres in de-ionized (DI) water. Care was taken to remove the surfactants of the commercial solution by

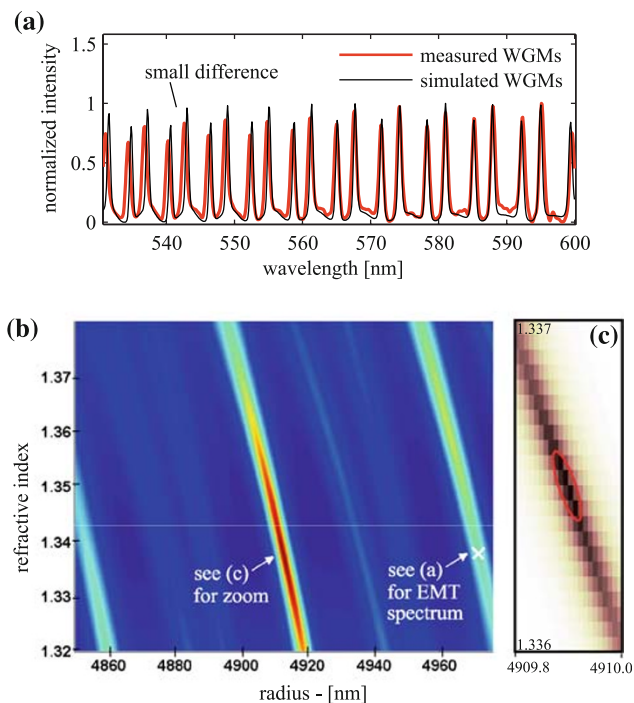


Fig. 3 **a** Same experimental spectrum as in Fig. 1c (red) superposed to the calculated EMT spectrum (black) 60 nm in radius away from the best fit. **b** Contrast enhanced χ^2 map of EMT calculated spectra compared to the experimental spectrum of Fig. 1c with the absolute minimum identified in red and zoomed in **c**. These maps are differently sampled than the set used in practice to give a clear view of the overall behavior

repeated centrifugation and resuspension. The resolution of the technique was evaluated from the standard deviation of (a^*, m_0^*) measured with 10 consecutive spectra taken on the same microsphere and yielded 0.1 nm for a^* and 0.0003 for m_0^* . Our technique was then applied on 100 different microspheres in DI water, and the measured refractive index was 1.3367 ± 0.0003 with radiuses ranging from 4,860 to 4,980 nm. In this case, the uncertainty on m_0^* has been estimated by bootstrapping on 10 groups of 10 samples; its value being the same as the single microsphere case, it shows the ergodicity of the sensor. The mean difference from the theoretical value of water (1.3325 ± 0.0001) [28] is then used as a constant offset to correct for a systematic error that likely comes from omitting the variation of m_0 with wavelength. This new sensor is now tested as a refractometer in Fig. 4 on water–ethanol and water–isopropanol solutions at different concentrations. Each point represents the average of 50 measures and is compared with reference curves [28]. At low alcohol concentration, the reference curves fall within the 99.7% confidence interval of our data points. However, there is a systematic deviation for higher alcohol concentrations. Though degradation in precision can be expected in this latter case due to a lower refractive index contrast at the

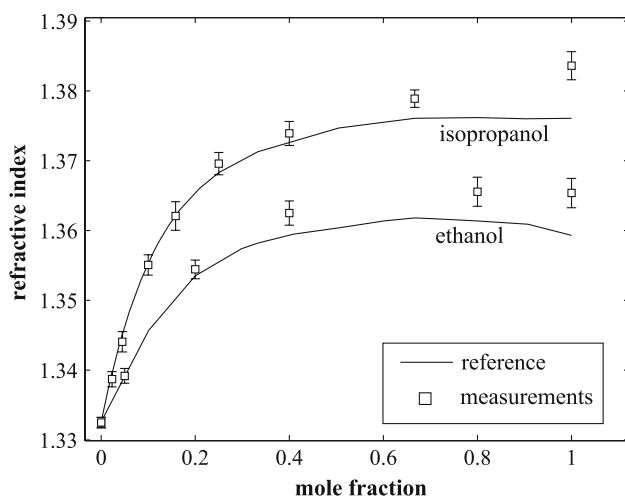


Fig. 4 Refractive index of different isopropanol and ethanol concentrations in water measured with our analysis of multiple WGMs. Spectra were acquired and analyzed for 50 fluorescent microspheres at each concentration, each point corresponds to the average of the refractive index distribution. The uncertainties represent the standard deviation of each distribution. The lines labeled reference in this case are measures taken with standard optical methods [28]

microsphere/solution interface reducing the visibility of the WGMs, we attribute the deviation mostly to the interaction of the polystyrene microsphere with its environment, since the alcohol can penetrate the microsphere and affect its optical properties. Swelling of polystyrene can occur as well in solutions with higher alcohol content, but this effect is accounted for independently by the algorithm adjusting automatically to the larger microsphere radius. Our demonstration of the technique here relies on convenient commercial microspheres as sensors that are not yet entirely optimized to reach the best resolution, thus work on the microcavity design is needed before comparing with the resolution of other sensors.

Biodetection

A different and promising application to this new technique is high capture cross section biodetection. Since microspheres are negatively charged with a zeta potential measured to be around -60 mV, they must be covered by a poly-L-lysine [29] polymer in order to attract negatively charged analytes such as spores and bacteria [30]. Purified *Bacillus atrophaeus subsp. globigii* (referred to hereafter as simply *B. globigii*) spores were prepared and counted as previously described [31]. These spores have an elongated shape with dimensions of approximately 2 by 1 μm . They are shown in Fig. 2b on a microsphere as observed with a 100X microscope objective. The spores were centrifugated from their PBS solution and resuspended in DI water at

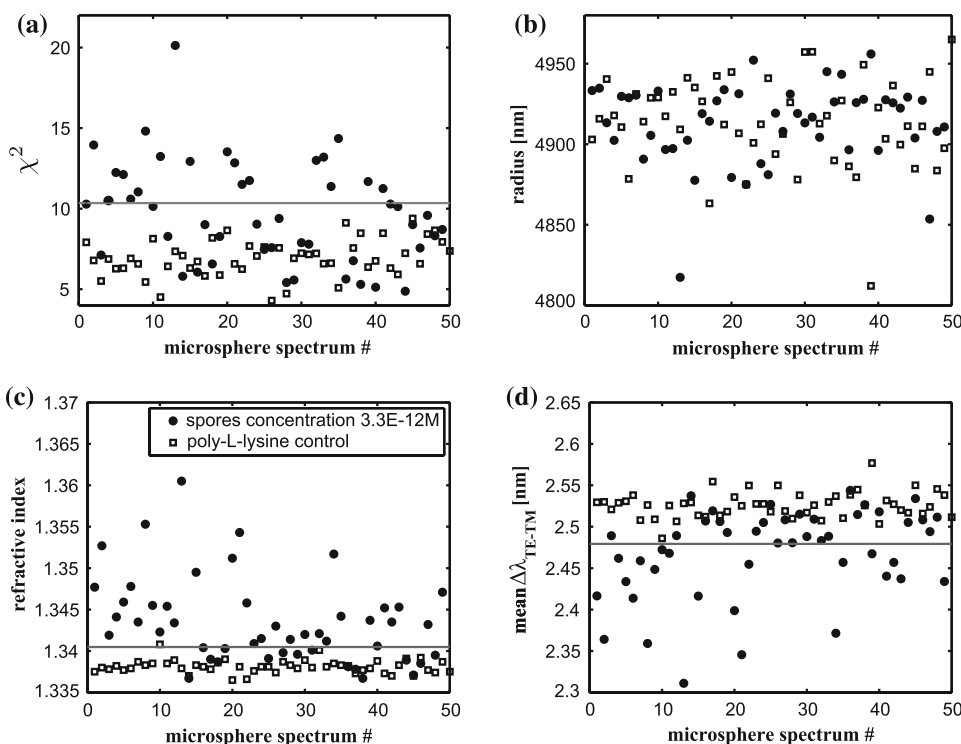
concentrations between 6.6×10^{-15} M (3.9×10^6 spores/ml) and 3.3×10^{-12} M (1.9×10^9 spores/ml).

We emphasize that no measures were taken on the microspheres prior to mixing them with *B. globigii* spores. The signal transduction mechanisms for biodetection here are not the experimental variations in the WGM spectrum of a single microsphere starting from an initial analyte-free solution as done commonly. Instead, we seek departures from the ideal case considered by the EMT, i.e., a perfectly spherical and evenly fluorescent microsphere within a homogeneous medium. Indeed, spores adsorbed on microspheres, or otherwise located within the evanescent field region (referred to hereafter as analyte capture), will perturb the WGM propagation in a more local manner than a homogeneous change in m_0 . The fitting algorithm will partially adapt to this perturbation by adjusting (a^* , m_0^*) which will no longer represent the microsphere radius and refractive index of water; hence in presence of analytes, we label (a^* , m_0^*) as apparent radius and apparent refractive index respectively. Nonetheless, the quality of the fit deteriorates as indicated in Fig. 5a by the higher absolute minimum χ^2 values we obtained, and this, in itself, is already an indicator that an inhomogeneous perturbation, not taken into account in our current model, occurs due to the *B. globigii* spores.

Since the microspheres' polydispersity hides the shift of apparent radius caused by the spores, Fig. 5b, we investigate the behavior of the apparent refractive index instead. Figure 5c shows the values obtained from 50 microspheres in the 3.3×10^{-12} M solution of *B. globigii* spores. We readily see that most of these values are significantly different from the refractive index of water. We also present in Fig. 5c the refractive indexes measured with 50 microspheres in a spore-free control sample containing poly-L-lysine coated microspheres in DI water that approach the ideal EMT case. This control sample allows us to estimate the effect of random fluctuations in experimental conditions, such as the thickness and surface roughness of the polymer coating, temperature, etc. These fluctuations also introduce departures from the ideal EMT case, but most of the apparent refractive indexes measured in the solution with spores are greater than the values from the control. This is in sharp contrast with the apparent radii values of Fig. 5b that fluctuates in the same manner for both solutions due to the microspheres' polydispersity. Our method thus successfully detects the presence of *B. globigii* spores and not only experimental artefacts, this without any requirements on the microspheres' polydispersity.

Going back to the EMT fitted spectrum, we can seek for a characteristic of the WGMs that isn't too sensitive to the randomly fluctuating microsphere radius but yet known to be correlated to the refractive index in the ideal homogeneous case. The spacing in wavelength between $TE_l - TM_l$

Fig. 5 **a** Goodness of fit χ^2 values, **b** microsphere apparent radii, **c** apparent refractive indexes and **d** mean TE-TM mode spacings obtained from the EMT fit on the WGM spectra of 50 fluorescent microspheres labeled on the x axis. The *black dots* are for a $3.3\text{E-}12\text{ M}$ ($1.9\text{E}9$ spores/ml) solution of *B. globigii* spores while the *open squares* are for the control sample in DI water. The *gray line* represents the threshold (3σ , 99.7% confidence interval) for biodetection occurring above the *line* in **(a)** and **(c)**, but below it in **(d)**



modes was shown to be such a characteristic [11], and we calculated its mean value for the $l \simeq 76$ to $l \simeq 85$ modes (mean $\Delta\lambda_{TE-TM}$) in our EMT fitted spectra. The results are shown in Fig. 5d for both the $3.3 \times 10^{-12}\text{ M}$ solution of *B. globigii* spores and the control sample. We combined the panels (c) and (d) of Fig. 5 into a new one: each point in Fig. 6 corresponds to a single microsphere EMT fitted spectrum whose coordinates are its apparent refractive index (x axis) and its mean TE-TM mode spacing (y axis). The anticipated correlation between both fitted parameters is clearly seen with some dispersion similar to the one observed for the control sample. The wider spread along the vertical direction is attributed to fluctuations in microsphere radii but is limited by the $< 5\%$ polydispersity stated by the manufacturer. Many other characteristics of the WGMs can be investigated to find the most relevant indicators of biodetection [32].

Interestingly, the solution with spores yields an elongated spread of data points. A possible interpretation for this elongation is that its (m_0 , mean $\Delta\lambda_{TE-TM}$) coordinates are related to the number of spores on a single microsphere. Data points in Fig. 6 with lower apparent refractive index, and its associated higher mean TE-TM mode spacing, are closer to the control sample and thus might correspond to fewer spores adsorbed on the microsphere. Conversely, data further away in the lower right of the graph are likely to represent microspheres with a greater number of adsorbed spores. This seems to be confirmed when we compare the elongation for 2 different spore

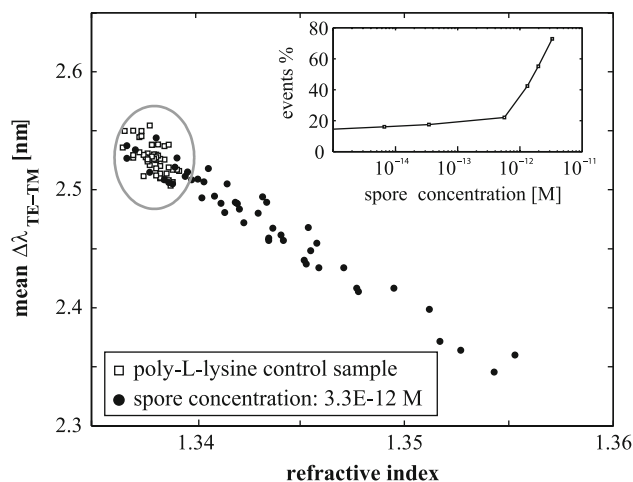


Fig. 6 Data of the previous figure for the $3.3\text{E-}12\text{ M}$ solution of spores and the control sample, but presenting the apparent refractive index on the x axis and the mean TE-TM spacing on the y axis to put emphasis on the correlation. The *gray ellipse* corresponds to the threshold set at three standard deviations, beyond which a data point is considered as a biodetection event. The *graph* in the inset shows the biodetection event percentage for distributions of 50 measurements at different concentrations of *B. globigii*. spores

concentrations in Fig. 7. The cloud of data points is less stretched out, more clustered in the upper left of the graph, when the solution contains fewer spores per unit volume consistent with a smaller number of spores adsorbed per microsphere.

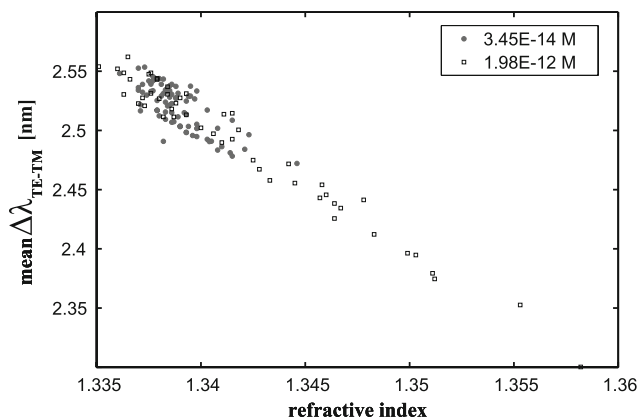


Fig. 7 Apparent refractive index and calculated mean TE-TM spacing of 50 microsphere sensor measurements for two different concentrations of *B. globigii* spores, 3.45E–14M and 1.98E–12M. The data for the higher concentration of spores stretch further into the lower right where we assume that each point corresponds to a greater number of spores adsorbed on the corresponding microsphere

To start quantifying the detection of *B. globigii* spores, we use the control sample as a reference and assume that no solvent contamination occurs. The threshold for bio-detection is set at 3 standard deviations from the average refractive index and mean TE-TM spacing values of the control sample. This threshold is represented by the gray ellipse in Fig. 6. All points lying outside this threshold are considered as detection events. When there are more spores in the solution, a larger fraction of the microsphere population will capture them corresponding to an increasing number of detection events. This relationship, as shown in the inset of Fig. 6, was measured using the solutions of known spore concentration. It can then become a quantitative reference curve to evaluate unknown spore concentrations with a measure of the biodetection event percentage. As the concentration of spores in solution increases, the detection event ratio will approach unity, but the data points should continue to move along the $(m_0, \text{mean } \Delta\lambda_{TE-TM})$ correlation curve. Hence, the sensor could still yield a reliable measure of spore concentration using the average of the apparent refractive index values instead, since this average will increase as the cloud of data points moves.

Coating Microspheres with cQDs

It is desirable to extend the fluorescence range of the microspheres, since the numbers of WGMs available for fitting and statistical analysis will be increased. This can be accomplished with cQDs of different emission colors mixed together and coated on the microspheres to provide the light source coupling into the WGMs. Other

improvements should ensue from replacing embedded organic fluorophores with cQDs, such as (1) broader absorption spectra giving more freedom for the choice of excitation wavelength; (2) better visibility of the WGMs, since cQDs located only on the microsphere surface have a better overlap with the evanescent field of the WGMs, thus increasing the coupling and reducing the spontaneous fluorescence background; and (3) it becomes possible to use silica microspheres with less permeability to the solvents and less internal light scattering than polystyrene, hence improving the Q factor.

The cQDs were prepared following an organo-metallic synthetic protocol, then were made water soluble by encapsulating them in an amphiphilic polymer, and finally were coated on the microspheres with a layer-by-layer (LbL) procedure. More details on these methods can be found elsewhere [17, 33]. Briefly for the encapsulation, the cQDs were transferred from chloroform to water in presence of soluble poly(styrene-co-vinyl benzyl chloride) copolymer previously quaternized with N,N dimethylhexadecylamine. The surface charge making the cQDs polar, hence water soluble, is provided by quaternary ammonium ions linked to the polymer. Since this charge is positive, the cQD coated microspheres will be ready to attract negatively charged analytes. For the LbL coating method, the first step consisted of the alternate adsorption of poly(ethyleneimine) (PEI) and polyacrylic acid salt (PAA) onto polystyrene microspheres in phosphate buffer saline solution. This primer layer provided a negatively charged microsphere surface. In a second step, the positively charged cQDs were electrostatically attracted on the negatively charged carboxyl (COO⁻) groups of PAA on the microspheres.

Preliminary results are shown in Fig. 8, and clear WGMs are observed in the fluorescence spectrum of green CdSe/ZnS cQDs coating $\approx 3 \mu\text{m}$ microspheres. Their spectral range of $\sim 100 \text{ nm}$ is already slightly larger than the emission range of the commercial microspheres previously studied even if this particular synthetic batch of cQDs was not optimized to cover a large emission bandwidth. Indeed, relaxing the growth conditions would easily yield more diverse cQD sizes and the overall emission spectrum would be broadened, since the cQD emission wavelength typically changes with their size. In upcoming experiments, we will coat the microspheres with mixed batches of cQDs emitting different large-bandwidth colors to broaden the spectrum even more, but here we are comparing the WGMs with those from the commercial microbeads on roughly the same green spectral range.

We first observe the expected decrease in spontaneous fluorescence background compared to the spectrum of the commercial microbeads, Fig. 2(a). This confirms the location of the cQDs near the microsphere surface, they

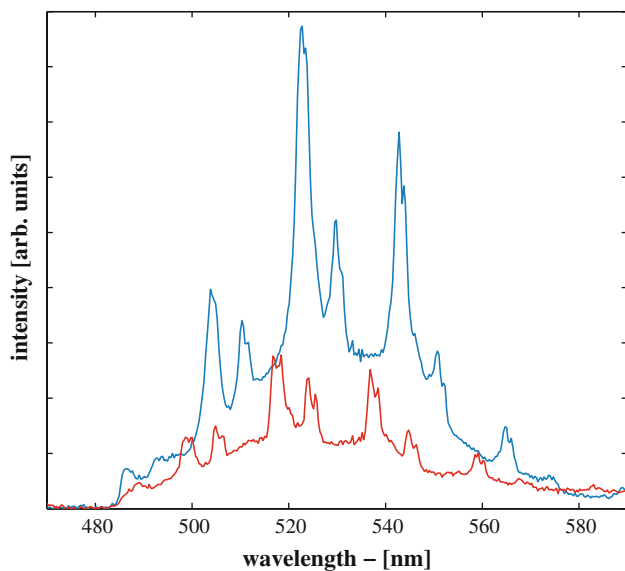


Fig. 8 WGMs in the fluorescence spectra of CdSe/ZnS cQDs coating $\approx 3 \mu\text{m}$ polystyrene microspheres. The spectra shown on the same scale are for two different microspheres. A small fluorescence background is observed as well as tiny peaks in each WGM. These peaks are attributed to polar modes, indicating that the spherical symmetry of the microspheres is broken

most likely stayed within the charged polymer layers without diffusing significantly. The EMT will thus need to be modified to account for the emitting dipoles that are now only in a spherical shell around the microsphere.

Another observation about the WGMs in Fig. 8 is their low Q factor of ≈ 200 associated with a wide spacing between the modes. This is not entirely attributed to the cQD coating, since the $\approx 1.5 \mu\text{m}$ microsphere radius is significantly smaller than the $\approx 4.95 \mu\text{m}$ radius of the commercial microspheres. Such a small microsphere radius was chosen to improve the detection sensitivity, since the WGMs' evanescent field leaks further out into the surroundings to be probed [34]. However, as was mentioned in Sect. 2, a compromise must be made between the Q factor and the free spectral range between the azimuthal l -numbered modes. With the current $\sim 100 \text{ nm}$ -wide spectra, the small number of WGMs will not be sufficient to make our fitting algorithm converge to a single absolute χ^2 minimum. This issue will be addressed by wider spectra emitted from multicolored cQDs coating slightly bigger microbeads.

A last observation, which was not seen in the case of the commercial microbeads, is the presence of tiny peaks within each azimuthal TE and TM mode more clearly seen in the red plot of Fig. 8. In fact, a large drop by a factor 10 of the Q factor for the cQD-covered microbeads compared to the commercial ones is surprising and is likely to come from the apparition of the extra peaks in addition to the

broadening of the azimuthal l -modes for smaller microspheres. This suggests the presence of an elongation breaking the symmetry of the microspherical cavity. Indeed, when the microbeads are perfectly spherical, the angular dependence of the electromagnetic field is symmetric and it yields a series of polar m -modes degenerate in wavelength for each l -mode. The extra peaks in the experimental spectra are presumably the polar modes no longer degenerate due to a small elongation $e = (r_p - r_e)/a$ where r_p is the polar radius and r_e the equatorial radius of the resulting spheroid. The polar m -modes can be spread over more than a nanometer by elongation values as small as 0.005 [35], which are even easier to reach in the case of microbeads with smaller radii a . The possible origins of this elongation here could be an uneven LbL polymer and cQD coating or simply the microbeads themselves if they were already distorted. Future work on cQD-covered microbeads will focus on raising the Q factor by improving the cQD deposition methods and the choice of material for the microspheres (silica, melamine formaldehyde, etc.) as well as adjusting our fitting algorithm for the modified EMT and for larger WGM spectra.

Conclusion

The results obtained for a polydisperse population of free floating fluorescent microspheres show that it is indeed possible to determine at the same time the microsphere size and its surrounding refractive index when multiple WGMs are used in the analysis of the emission spectrum. We have thus developed a calibration-free refractive index sensor and tested it on different water–alcohol solutions. A precision of 3×10^{-4} in refractive index measurement was achieved and could be improved, since it is proportional to the number of spectra acquired and to the spectral range used. We also demonstrated the versatility of our method by applying it to biodetection. *B. globigii* spores were successfully detected with two different parameters in the WGM analysis, i.e., the apparent refractive index and the calculated mean TE-TM mode spacing; the correlation between them was also verified. This biodetection method is easy to implement with a small number of preparation steps and only requires low-cost equipment. A freely moving population of microsphere sensors will also increase analyte capture efficiency compared to a static sensor made of immobilized microspheres or other surface-based detection methods. These features combined with the systematic character of our method offer a possibility for automatization in real time, especially when the microsphere sensors are coated with colloidal quantum dots of various colors to improve the WGM visibility and provide a wide fluorescence spectrum.

Acknowledgments This research was supported by the Fonds québécois de la recherche sur la nature et les technologies (FQRNT). The authors would like to thank P. Laroche for technical support, A.P. Mosk for helpful communications and D. Barnett for a starting point on a function in the code.

Open Access This article is distributed under the terms of the Creative Commons Attribution Noncommercial License which permits any noncommercial use, distribution, and reproduction in any medium, provided the original author(s) and source are credited.

References

1. K.J. Vahala, *Nature* **424**, 839 (2003)
2. C.F. Bohren, D.R. Huffman, *Absorption and Scattering of Light by Small Particles* (Wiley-VCH, New York 1998)
3. A.N. Oraevsky, *Quantum Electron.* **32**, 377 (2002)
4. N.M. Hanumegowda, C.J. Stica, B.C. Patel, I. White, X. Fan, *Appl. Phys. Lett.* **87**, 201107 (2005)
5. A.M. Armani, R.P. Kulkarni, S.E. Fraser, R.C. Flagan, K.J. Vahala, *Science* **317**, 783 (2007)
6. F. Vollmer, S. Arnold, *Nat. Meth.* **5**, 591 (2008)
7. F. Vollmer, S. Arnold, D. Keng, *PNAS* **105**, 20701 (2008)
8. S. Arnold et al., *Opt. Express* **17**, 6230 (2009)
9. Y. Lin et al., in *Laser Resonators and Beam Control IX*. Biochemical Detection with Optical Whispering-Gallery Resonators, vol 6452 (SPIE, San Jose, 2007), pp. 64520U–8
10. A. Weller, F. Liu, R. Dahint, M. Himmelhaus, *Appl. Phys. B* **90**, 561 (2008)
11. P. Zijlstra, K.L. van der Molen, A.P. Mosk, *Appl. Phys. Lett.* **90**, 161101 (2007)
12. R.E. Benner, P.W. Barber, J.F. Owen, R.K. Chang, *Phys. Rev. Lett.* **44**, 475 (1980)
13. E. Nuhiji, P. Mulvaney, *Small* **3**, 1408 (2007)
14. D. Morrish, X. Gan, M. Gu, *Appl. Phys. Lett.* **81**, 5132 (2002)
15. U. Woggon et al., *Appl. Phys. B* **77**, 469 (2003)
16. X. Fan, P. Palinginis, S. Lacey, H. Wang, M.C. Lonergan, *Opt. Lett.* **25**, 1600 (2000)
17. C.Ni. Allen et al., Nanocrystal coated beads for optical coding and whispering gallery modes, in *Proceedings of SPIE*, Ottawa, 2007, pp. 67962Z–67962Z–14
18. Y.P. Rakovich et al., *Phys. Status Solidi (C)* **2**, 858 (2005)
19. D. Morrish, X. Gan, M. Gu, *Appl. Phys. Lett.* **88**, 141103 (2006)
20. N. Gaponik et al., *Nanoscale Res. Lett.* **1**, 68 (2006)
21. S. Pang, R.E. Beckham, K.E. Meissner, *Appl. Phys. Lett.* **92**, 221108 (2008) PMC2682744
22. S. Pang, K.E. Meissner, G.L. Cote, A.V. Priezhev, in *Optical Diagnostics and Sensing VIII*. Tagless Remote Refractometric Sensor Based on WGMs in Quantum Dot-Embedded Microspheres, vol 6863 (SPIE, San Jose, 2008), pp. 686303–12
23. A. Francois, M. Himmelhaus, *Appl. Phys. Lett.* **94**, 031101 (2009)
24. A. Francois, S. Krishnamoorthy, M. Himmelhaus, Advances in label-free optical biosensing: direct comparison of whispering gallery mode sensors with surface plasmon resonance, in *Proceedings of SPIE*, San Jose, 2008, pp. 686211–686211–7
25. H. Chew, *Phys. Rev. A* **38**, 3410 (1988)
26. H. Chew, *J. Chem. Phys.* **87**, 1355 (1987)
27. D. Marquardt, *SIAM* **11**, 431 (1963)
28. J. Herraes, R. Belda, *J. Solut. Chem.* **35**, 1315 (2006)
29. H. Ren, F. Vollmer, S. Arnold, A. Libchaber, *Opt. Express* **15**, 17410 (2007)
30. H. Douglas, *J. Appl. Bacteriol.* **20**, 390 (1957)
31. F.J. Picard et al., *J. Clin. Microbiol.* **47**, 751 (2009)
32. M. Charlebois et al., Parameter study of WGM biodetection with an instantaneous spectrum of a fluorescent microsphere, (to be published)
33. C.Ni. Allen, N. Lequeux, C. Chassenieux, G. Tessier, B. Dubertret, *Adv. Mater.* **19**, 4420 (2007)
34. S. Arnold, M. Khoshima, I. Teraoka, S. Holler, F. Vollmer, *Opt. Lett.* **28**, 272 (2003)
35. Y.P. Rakovich, J.F. Donegan, A.L. Rogach, in *Hybrid Nanocomposites for Nanotechnology*. Photonic Structures of Luminescent Semiconductor Nanocrystals and Spherical Microcavities (2009), pp. 653–703